Bull Volcanol (2001) 63:227–237
DOI 10.1007/s004450100137

RESEARCH ARTICLE

Richard J. Stevenson † · Donald B. Dingwell
Nikolai S. Bagdassarov · Curtis R. Manley

Measurement and implication of "effective" viscosity for rhyolite flow emplacement

Received: 6 August 2000 / Accepted: 10 February 2001 / Published online: 17 May 2001

Abstract Hazardous explosive activity may sporadically accompany the extrusion of silicic lava domes. Modelling of the emplacement of silicic domes is therefore an important task for volcanic hazard assessment. Such modelling has been hampered by a lack of a sufficiently accurate rheological database for silicic lavas with crystals and vesicles. In the present study, the parallel-plate viscometry method was applied to determine the shear viscosity of five natural rhyolitic samples from a vertical section through the Ben Lomond lava dome, Taupo Volcanic Centre, New Zealand. Rheological measurements were performed at volcanologically relevant temperatures (780–950°C) and strain rates (10^{-5}–10^{-7} s^{-1}). Although these samples are in the metastable state, viscosity determinations, melt composition, as well as water and crystal contents of samples were demonstrably stable during experiments. For samples containing up to 5 vol.% microlites, the composition of the melt, rather than the physical effect of suspended crystals, had greater influence on the effective viscosity of the silicic magma. Samples with 10 vol.% microlites and containing a flow banding defined by microlites show no significant orientational effects on apparent viscosity. The rheological measurements were used together with a simple cooling model to construct thermal and viscosity profiles revealing conditions during the emplacement of the Ben Lomond lava dome.

Keywords Rhyolite · Lava flow · Viscosity · Pumice · Arrhenius dependence · Cooling model · Vesiculation

Editorial responsibility: T.H. Druitt
† Deceased

R.J. Stevenson · D.B. Dingwell
Bayerisches Geoinstitut, Universität Bayreuth,
95440 Bayreuth Germany

N.S. Bagdassarov (✉)
Institut für Meteorologie und Geophysik,
J.W. Goethe Universität-Frankfurt, Feldbergstrasse 47,
60323, Frankfurt am Main, Germany
e-mail: nickbagd@geophysik.uni-frankfurt.de
Tel.: +49-69-79823376, Fax: +49-69-7982380

C.R. Manley
52 158th Place NE, Bellevue, WA 98008–4314 USA

Present address:
D.B. Dingwell, Institut für Mineralogie,
Petrologie und Geochemie, Universität München,
Theresienstrasse 47/III, 80333 Munich, Germany

Introduction

The emplacement of silicic lava flows and of the Pacific Rim over the past decade has focused interest and attention on the potential hazards associated with these volcanoes. Explosive activity may precede or accompany the extrusion of lava. The distribution of vesicular textures on silicic lava flows has been related to their likelihood of experiencing explosive behaviour during flow advance (Fink and Manley 1989; Fink et al. 1992), and variations in vesicularity are, in part, related to variations in volatile contents (Westrich et al. 1988; Anderson and Fink 1990). Some lava flows contain explosion craters indicating high internal pressures in these flows (Anderson and Fink 1992; Fink et al. 1992), caused by crystallisation and the resultant build-up of excess pressure in the interior of the flow (Sparks 1997). Also, flow-front collapse can generate pyroclastic flows (Anderson and Fink 1990; Anderson et al. 1995; Jousset and Okada 1999; Matthews et al. 1997; Mothes et al. 1998; Richter et al. 1994; Swanson and Holcomb 1990; Wadge et al. 1995; Watanabe et al. 1999; Yamashina and Shimizu 1999), as observed at active dacitic lava domes such as Lascar and Socompa volcanoes in northern Chile, Usu–Hokkaido and Unzen in Japan, Cotopaxi in Ecuador, Santiaguito in Guatemala, Mount Drum in Alaska, and Mount St. Helens in the U.S. The formation of explosion pits and pyroclastic flows are the two most significant volcanic hazards associated with viscous silicic lava flows.

Despite its obvious importance for risk assessment, previous modelling of silicic flows has been hampered by an insufficient rheological database on lavas for input

into eruption models. Also, very recently, questions have been raised concerning the accuracy of empirical models which predict the effect of water on the viscosity of rhyolitic and andesitic melts (Dingwell et al. 1996; Richet et al. 1996; Hess and Dingwell 1996; Schulz et al. 1996; Scaillet et al. 1996). As a first approximation, some physical properties can be deduced from detailed physical and textural studies of lava flow carapaces (Fink 1983) or from sections bisecting the thickness of flows (Stevenson et al. 1994). More recently, however, viscosity has been measured for natural rhyolitic obsidians at volcanologically relevant temperatures and strain rates (Stevenson et al. 1995, 1996). This new type of data permits much more accurate modelling of the rheological properties of silicic flows.

We studied a silicic lava dome in New Zealand, the Ben Lomond dome, Taupo Volcanic Centre. Viscosity measurements on natural samples taken from specific lava flow facies, together with a simple cooling model, were used to constrain the timing of formation of the textural units. These results are useful for volcanic hazards assessment for this and other, similar calc-alkaline lava flows.

The Ben Lomond flow

The Ben Lomond dome (ca. 100 ka) consists of two flow lobes up to 3.5 km in length, bisected by a fault scarp that exposes up to two-thirds of the internal flow stratigraphy (Fig. 1a). This lava flow consists of an eroded finely vesicular pumice carapace (Fig. 1b, FVP), an upper obsidian layer (U.OBS) cross-cut by a pumicious breccia and a spherulitic transition zone (TZ) into crystalline rhyolite (RHY; for more details see Stevenson et al. 1994). The base of the flow is not exposed, as valleys between flow lobes are filled by pumice alluvium. Almost all the FVP layer has been eroded, and the flow is covered by a 22-ka ignimbrite. Near the margins of the flow lobes, flow layering ramps upward, steepening in dip from 30 to 80° toward the surface. The inferred vent position is near the summit of the lava dome, based on flow banding orientation and the surface slope of the lava lobes.

This flow was chosen for rheological modelling because it: (a) has been adequately documented in the literature in terms of its stratigraphy (Stevenson et al. 1994) and its composition and microstructural features (Sharp et al. 1996); (b) contains both near-surface and internal sections of the flow; and, most importantly, (c) it contains fresh non-hydrated, unweathered rhyolitic obsidian ranging from aphyric to containing ca. 10 vol.% microlites, making it well suited to high-precision viscosity measurements using the parallel-plate method.

Sample description

Viscosity measurements were performed on five natural samples: one pumice (BLP) and four obsidians (BL3, 4,

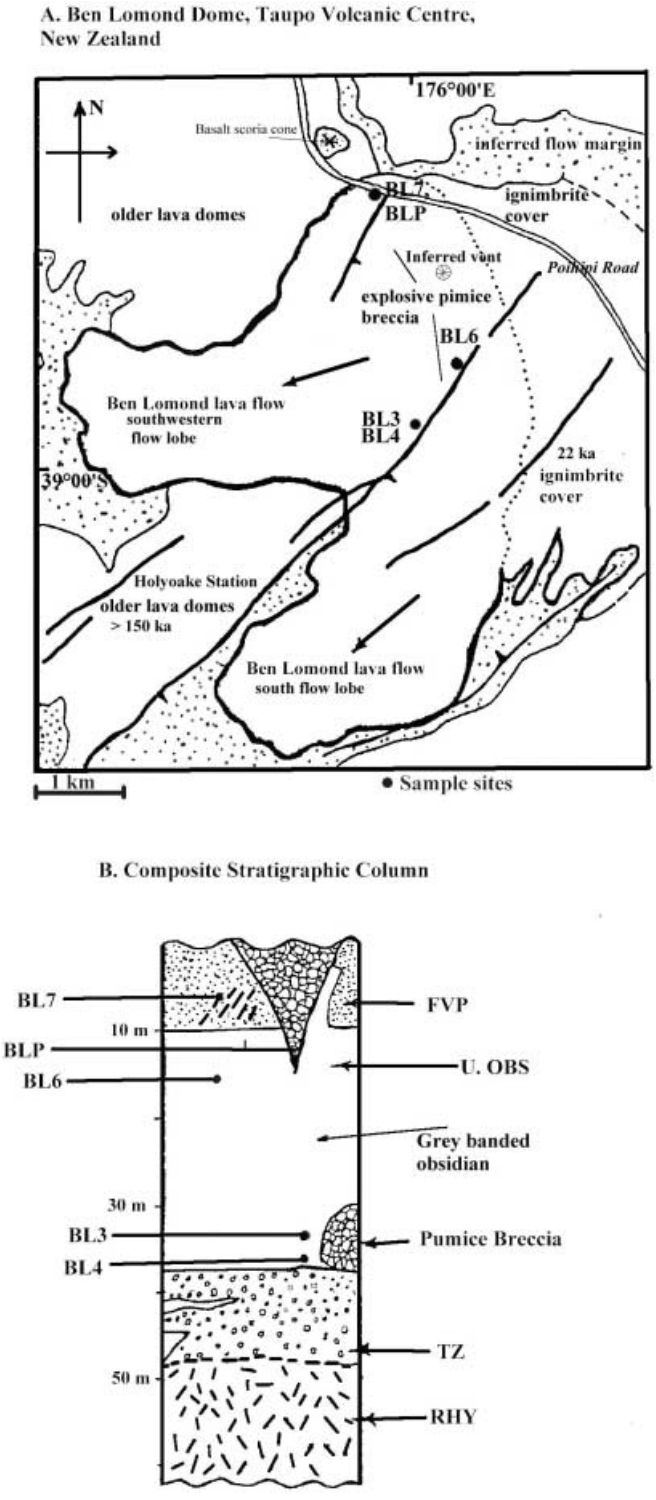

Fig. 1 Morphology of **A** the Ben Lomond Dome and **B** a stratigraphic column with sampling sites. *FVP* finely vesicular pumice; *U. OBS* upper obsidian layer; *TZ* spherulitic transition zone; *RHY* crystalline rhyolite layer. Stratigraphic units are in metres (redrawn from Stevenson et al. 1994)

6, 7). The stratigraphic locations of these samples are shown in Fig. 1b. In addition, viscosity measurements were performed on one sample (BL6-r) re-fused at 1650°C to remove water, and one sample hydrothermally treated so as to contain 0.5 wt.% H_2O. These experiments were necessary in order to better constrain the viscosity of the melt phase with varying water contents for the vesicular pumiceous samples.

Natural samples

Sample BL7 is a platy obsidian clast collected from FVP (finely vesicular pumice) within the exposed upper 6 m of the lava flow carapace. Individual clasts are less than 0.36 m size and comprise aphyric, non-spherulitic black obsidian with striated surfaces and rare bubble-rich internal layers. Microlite content is <0.2 vol.% consisting of strings of Fe–Ti oxides and opx–cpx rods.

A black aphyric obsidian (sample BL6) was collected within the upper 5 m of the upper obsidian layer (U. OBS in Fig. 1b). This sample is sparsely spherulitic and microlite-poor with <0.5 vol.% microlites of rod-like shape (10×1 μm size), stringer and spider-like form. Rare microphenocrysts (<40 μm width) occur comprising magnetite, augite, amphibole and tabular plagioclase laths of 60×30 μm average size.

Sample BL3 is grey-banded obsidian collected approximately 15 m below BL6 (ca. 30–35 m below the flow surface). BL3 contains up to 8 vol.% crystals (average ca. 5 vol.%) which occur in several populations:

1. Microphenocrysts <1.2 μm width (as described above for BL6)
2. Rod-like microlites with aspect ratio of 10–15, and average length of 16 μm (<0.6 μm width)
3. A smaller population of crystals <0.6 μm in width, termed “nanolites” by Sharp et al. (1996).

BL4 was collected within 1 m of BL3. The hand specimen contains a microlite-rich flow band 3 cm width with ca. 10 vol.% flow-aligned microlites homogeneously distributed within the flow band. In addition, the sample is characterised by a larger proportion of plagioclase laths compared with BL3.

White and pale pink pumiceous blocks occur as a pod-like outcrop at an equivalent depth of 30–35 m below the surface. These pumiceous blocks comprise a clast-supported breccia which also occurs as an inverted cone-shaped outcrop cross-cutting the U. OBS and FVP near the flow surface. Individual clasts average 120 mm length and attain 1.2 m in size. This outcrop is interpreted as a pumiceous breccia associated with explosion pit formation (Stevenson et al. 1994). Experimental samples (designed BLP) were derived from the pumice of the cone-shaped outcrop. The samples had an average vesicularity of 50 vol.% elongate vesicles with average apparent aspect ratios of 5–10 and an average vesicle diameter of ca. 10 μm. This textural type is entirely microlite-free.

Preparation of annealed and hydrated samples

In order to prepare an essentially dry rhyolite melt, chips (ca. 5 mm size) of BL6 were vesiculated at 1300°C for a few minutes followed by cooling and crushing to a fine grain powder. The powder was incrementally annealed in a Pt-crucible for several hours at 1650°C followed by slow cooling to room temperature over 24 h (Stevenson et al. 1998). The end product (BL6-r) contained no crystals, no bubbles, and had a water content of ca. 0.03 wt.% measured by FTIR. This formed the starting material for the synthesis of a hydrous BL6 melt. Powdered BL6-r was added to a Pt-capsule, the equivalent of 0.5 wt.% distilled water was added, and then the capsule was sealed by arc-welding. The capsule was examined for possible leakage by testing for weight loss after drying in an oven at 150°C for at least 1 h. Oven drying also ensured that the water (as vapour) was evenly distributed throughout the capsule. The hydrated melt was synthesised in an internally heated pressure vessel (CRSCM, Orléans, France) at 1300°C in excess of 3 kbar pressure for ca. 65 h (for method details see Roux et al. 1994). The end product was a bubble-free glass. All samples were held at 100°C during at least 1 h before rheological experiments in order to remove the absorbed water.

Methodology of viscosity measurements

For the natural samples and BL6-r, experimental viscosity determinations were performed in a vertical push-rod dilatometer, described previously by Bagdassarov and Dingwell (1992) and Stevenson et al. (1998), using the parallel-plate method (Gent 1960; Fontana 1970). Cylindrical samples (diameter 8 mm, length ca. 10 mm) were drilled from hand specimens, and the cylinder ends were ground flat and parallel. Samples of BL4 were drilled within a flow band parallel and perpendicular to flow-band orientation and microlite long axes. Microlites were distributed homogeneously within this sample. Coherent cylinders could not be drilled from samples of the FVP unit (BL7) because of the small size of obsidian clasts. Experimental samples of FVP (BL7) were heated to the temperature of interest at a rate of 10 K min^{-1}, then deformed by up to 10% of their initial length between two parallel plates of Al_2O_3 Frialit-Degussit (Germany). Previous measurements of shear viscosity on NBS 711 standard melt and comparison with tabulated data (e.g. Bagdassarov and Dingwell 1992), as well as parallel-plate viscometry on a remelted and anhydrous rhyolite (annealed for several hours at 1650°C), have shown that shear viscosity η_s is reproducible to within 0.07 $\log_{10}$ units Pa s. For the experimental stresses 10^3–10^5 Pa, strain rates 10^{-5}–10^{-7} s^{-1} are at least three orders of magnitude lower than those at which non-Newtonian behaviour is expected to occur for rhyolite melts (Webb and Dingwell 1990a, 1990b), and no strain-rate or stress-dependent rheology was observed.

Parallel-plate viscometry of viscous melts is possible within the range 10^8–10^{11} Pa s. Over most of this experi-

mental range, significant crystal growth/dissolution and bubble growth does not occur during the timescale of these experiments. When natural obsidians containing 0.1 and 0.2 wt.% water, originating from near-surface levels, are heated (at 1 bar) to temperatures >100°C above the glass transition, vesiculation can occur (Bagdassarov et al. 1996; Stevenson et al. 1997). Preliminary experiments were required to determine the "operating window" of temperature for viscosity measurements. The lower temperature limit results from the relaxation effect at viscosities higher than 10^{11} Pa s, and the upper temperature limit is determined by the temperature where vesiculation and expansion of the sample occurs within the experimental time scale of several hours. An "operating window" is defined as that temperature range above the glass transition in which no measurable drifts in sample chemistry or texture occur on the timescale of the experiment.

After determination of the "operating window" for each sample, the natural samples were heated to the required temperatures at a constant rate of 10 K min^{-1} and then held at a constant temperature as a series of loads were applied following a load and unload procedure previously described by Bagdassarov and Dingwell (1992) and Stevenson et al. (1998).

For hydrated sample BL6 the micropenetration method was used to determine viscosity (for method details see Pocklington 1940; Tobolsky and Taylor 1962). In order to accurately measure viscosity in a glass sample containing water, the duration of the experiment should be much shorter than the bubble nucleation time. The precision of the method depends on how robust the fitting of the depth-penetration curve to the theoretical dependence is (see discussion of this method in Stevenson et al. 1997).

In addition, the heat capacities of two natural obsidian samples BL3 and BL6 were measured in a differential scanning calorimeter (Setaram DSC 111) during cooling and reheating at four matching rates between 4 and 12 K min^{-1} (Stevenson et al. 1995). The derived heat capacity curves on these glassy samples were used to identify the glass transition temperature, which is dependent on the heating rate. To test any compositional drift in the samples during the course of experiments, chemical compositions were analysed on both pre- and post-viscometry samples using ICP-AES and electron microprobe. Water contents were measured by FTIR for all samples before and after viscosity experiments following methods in Stolper (1982) and Newman et al. (1986) at BGI (Bayreuth, Germany). Additionally, energy dispersive analysis on TEM was used for accurate determination of glass composition of the microlite-bearing BL3 sample (Sharp et al. 1996).

Experimental results

Composition and water contents

Chemical composition and water contents of the Ben Lomond samples are listed in Table 1. It has been demonstrated that bulk compositions are essentially homogeneous throughout the flow (Stevenson et al. 1994). Chemical bulk compositions of natural and remelted BL6 and BL6-r are identical except for water (Stevenson et al. 1998).

The FTIR measurements show that water loss was negligible during viscosity measurements. In addition, optical microscopic analysis showed that microlite contents remained constant within error before and after viscometry (Stevenson et al. 1995, 1996, 1998). The pale-pink pumice samples (BLP) were orange after parallel-plate viscometry. Although the composition of the sample remained the same during experiments, some oxidation may have occurred as oxygen species remnant from vesicles diffused form into the melt matrix of the sample. Near the free surface the oxidation may be controlled by the diffusion of Fe^{2+} cations to the vesicle surface and a counter flux of positrons into interior of glass (Cook and Cooper 2000). Even so, no drift in viscosity was recorded over the 4 h duration of the experiment.

Table 1 Chemical analyses of Ben Lomond samples. *n.d.* Not determined

Oxide	BL7 XRF	BL6 ICP-AES	BL6 remelted ICP-AES	BL3 glass TEM[a]	BLP XRF
SiO_2	77.06	77.48 (0.2)	77.53 (0.4)	77.88 (0.56)	77.03
TiO_2	0.18	0.17 (0.6)	0.17 (0.6)	0.16 (0.9)	0.19
Al_2O_3	12.50	12.2 (1.1)	12.17 (0.3)	12.03 (0.2)	12.74
FeO_t	1.4	1.3 (0.9)	1.3 (0.3)	1.19 (0.17)	1.44
MnO	0.05	0.05 (0.9)	0.05 (0.6)	0.05 (0.05)	0.05
MgO	0.24	0.17 (0.2)	0.17 (0.9)	0.05 (0.13)	0.23
CaO	1.11	1.14 (0.6)	1.13 (0.3)	1.06 (0.13)	1.1
Na_2O	4.01	3.9 (0.8)	3.89 (0.3)	3.64 (0.3)	3.69
K_2O	3.46	3.6 (0.7)	3.6 (0.7)	3.88 (0.34)	3.52
P_2O_5	0.02	n.d.	n.d.	0.01 (0.06)	0.02
Total[b]	99.61	100.63	100.22	100.00	99.78
H_2O	0.124	0.132	0.036	n.d.	3.12[c]

[a] For microlite-bearing BL3 sample TEM energy dispersive analysis of the glass between microlites is listed (Sharp et al. 1996). Analytical uncertainties 1 σ are in parentheses
[b] Total of original analysis: all other values are normalised to volatile-free conditions
[c] LOI (loss on ignition) value (105–1000°C); otherwise, water determined as total water by FTIR

Table 2 Viscosity data

Sample	T (°C)	logη (Pa s)
BL6	915	8.50 (0.06)
	879	9.10 (0.07)
	854	9.51 (0.04)
	820	10.05 (0.04)
	820	10.25 (0.05)
	788	10.62 (0.06)
BL7	807.5	10.24 (0.09)
	820	10.07 (0.05)
	844	9.68 (0.03)
	870	9.24 (0.05)
	883	9.19 (0.05)
BL3	915	8.88 (0.02)
	905	9.13 (0.03)
	891	9.31 (0.02)
	880	9.54 (0.03)
	875.6	9.48 (0.08)
	868	9.75 (0.05)
	848	10.03 (0.08)
	843	10.21 (0.05)
	819	10.50 (0.09)
	801	10.73 (0.02)
BL4 (perpendicular to flow banding)	860	10.14 (0.07)
	880	9.87 (0.05)
	893	9.65 (0.07)
	910	9.32 (0.02)
BL4 (parallel to flow banding)	867	10.11 (0.08)
	880	9.99 (0.06)
	894.5	9.68 (0.06)
	917	9.27 (0.06)
	948.5	8.91 (0.02)
BLP explosive breccia pumice	881	10.74 (0.06)
	900	10.42 (0.08)
	914	10.10 (0.09)
	925	10.02 (0.07)
	929.5	9.85 (0.06)
	954	9.72 (0.09)
BL6-r (remelted)	861	10.07 (0.02)
	879	9.81 (0.04)
	886	9.62 (0.04)
	905	9.34 (0.04)
	914	9.09 (0.03)
	923	9.04 (0.03)
	951.5	8.62 (0.02)
BL6-hydrated[a]	650	11.13 (0.01)
	664	10.76 (0.005)
	678	10.51 (0.005)
	697	10.19 (0.001)
	717	9.77 (0.006)

[a] Viscosities were measured by the micropenetration method; for details see Stevenson et al. (1997). Experimental uncertainties 1 σ are in parentheses

Fresh glass within the flow also enabled estimates of water content by Karl Fischer methods (ca. Westrich 1987). From loss on ignition estimates (LOI at 500–1000°C), the pumiceous sample (BLP) contains ca. 0.5 wt.% water, assumed to be mainly H_2O^+ as OH^- groups structurally bound within Si–O polymers with a maximum loss by pyrolysis at 600°C. From Karl Fischer titrations, the total water content from obsidians decreases from 0.1±0.01 wt.% proximal to the inferred vent to 0.08 and 0.06 wt.% for more distal sections on the flow margins, 2.5 and 2.8 km SE and SW, respectively. Bulk XRF determinations show that Cl and F occur in trace amounts of 900 and <150 ppm, respectively (Stevenson et al. 1994). Pre-eruptive volatile contents were not estimated because there are no melt inclusions in phenocrysts to analyse, or fresh juvenile obsidian clasts within a pre-dome tuff.

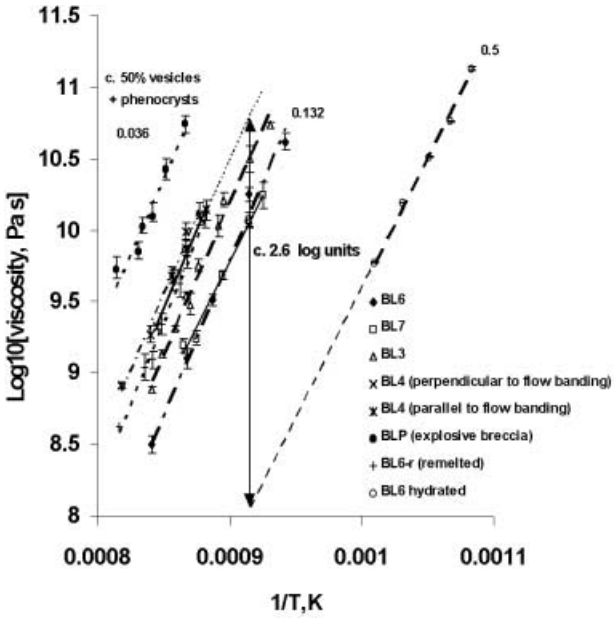

Fig. 2 Viscosity measurements of the Ben Lomond samples. *Numbers* indicate the water content of samples in weight percent. *Arrow* shows the difference between hydrated to 0.5 wt.% of water and remelted "dry" sample BL6. At temperatures 800–820°C, the difference may be as high as 2.6 orders of magnitude

Viscosity

Viscometry results on all samples are listed in Table 2 and plotted in Fig. 2. Over the viscosity range 10^8–10^{11} Pa s, the temperature dependence for these melts is Arrhenian with the following form:

$$\log_{10}\eta_S = \log_{10} A_\eta + \frac{E_\eta}{2.303RT} \quad (1)$$

where η_s is the shear viscosity at $T(K)$, and A_η and E_η are the pre-exponential factor and the activation energy of viscous flow, respectively, and R=8.314 J mol^{-1} K^{-1} is the gas constant. Values for A_η and E_η are listed in Table 3.

Scanning calorimetry

The glass transition temperature T_g for enthalpy relaxation can be obtained from the peak in the heat capacity curve in a sample cooled at a rate q. The dependence of

Table 3 Pre-exponential factor and activation energies of shear viscosity

Sample	$\log_{10}A_\eta$	E_η (kJ/mol)
BL6	–8.709 (0.57)	392.2 (11.9)
BL7	–6.742 (0.056)	351.3 (20.9)
BL3	–8.883 (0.065)	405 (14.4)
BL4 (⊥ to flow banding)	–9.247 (0.04)	421 (28)
BL4 (|| to flow banding)	–8.814 (0.06)	413.5 (24.6)
BLP explosive breccia	–6.557 (0.117)	381.2 (56)
BL6-r (remelted)	–9.927 (0.05)	434 (18.6)
BL6-hydrated	–8.265 (0.05)	342 (15.5)

1 σ error in parentheses

T_g on heating and cooling rates for silicate melts obeys the Arrhenian relationship with the following form:

$$-\log_{10}|q| = \log_{10} A_H + \frac{E_H}{2.303RT_g}, \quad (2)$$

where q is cooling rate in K/s, and A_H and E_H the pre-exponential factor and activation energy for enthalpy relaxation, respectively (e.g. Stevenson et al. 1995).

Both shear stress (viscometry) and enthalpic (calorimetry) relaxations are approximated to be Arrhenian over the investigated temperature and viscosity range. Activation energies defined by both methods are equal E_H=E_η (Stevenson et al. 1995). This permits the cooling rate of a natural sample to be calculated, if the viscosity at peak temperature (from heat capacity or dilatometric curves) is determined:

$$\log_{10} q = K - \log_{10} \eta_s(T_q), \quad (3)$$

where viscosity is in Pa s, q is in K s^{-1}. The value of K is set to 11.3 if the onset of the scanning calorimetry peak is taken as T_g (see Scherer 1984), or to 10.49 if the peak temperature in the calorimetry scan is taken as T_g (see Stevenson et al. 1995). The glass transition temperature range spans approximately 50–70 K depending on the particular thermal treatment used and the temperature dependence of the shear viscosity. If the cooling rate varies by a factor of four, a 25 K variation in the peak temperature or T_g is observed (Stevenson et al. 1995). Another method to estimate T_g is to use the onset of the peak on a scanning curve for heat capacity or volume expansion (Scherer 1984). The difference in the cooling rate estimation is discussed below, and T_g measured as function of laboratory cooling rate are presented in Fig. 3.

Effect of microlites and bubbles on apparent viscosity

The presence of crystals and bubbles influence the viscosity of magmatic suspensions (Dingwell et al. 1993). Based on experimental data in Fig. 2 and Table 2, the physical effect of up to 10 vol.% microlites, their shapes, and of 50 vol.% vesicles on the effective viscosity of magmatic suspensions can be evaluated.

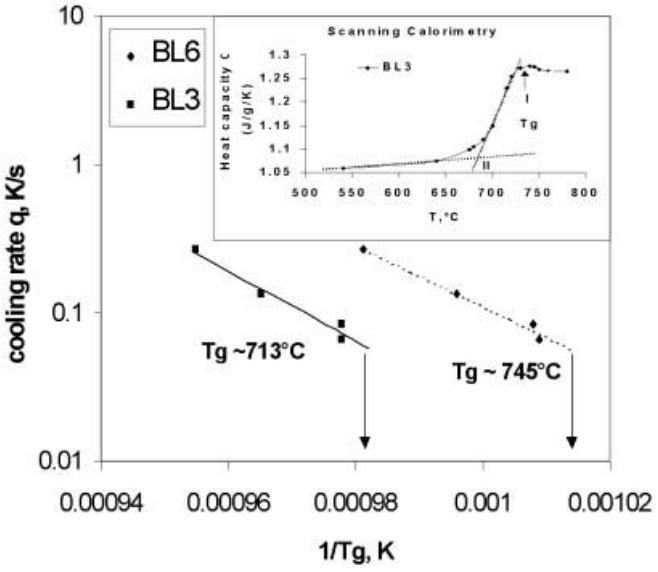

Fig. 3 Calorimetric data on the Ben Lomond samples. *Arrows* indicate the *Tg* obtained on raw samples without preliminary heating/cooling treatment. *Inset* demonstrates two methods for evaluation of T_g: from the peak temperature (I); and from the extrapolated onset of the peak on the scanning calorimetry curve (II)

BL6 vs BL3

Bulk compositions (from electron microprobe and XRF analyses) of BL6 and BL3 are the same (Table 1). However, TEM energy dispersive analysis of glass composition (Table 1), and scanning calorimetric data with matched quench rates (Fig. 3), indicate that the viscosity difference between BL6 and BL3 is almost entirely due to small changes in melt composition (Fig. 2). Owing to crystallisation of microlites within BL3, the resulting change in melt composition significantly outweighs any physical effect (<0.2 log units) of 5 vol.% suspended crystals contributing to the effective viscosity of the magma (Stevenson et al. 1996). This explaines why T_g of these two samples differs by almost 30°.

Sample BL4

In comparison with BL3, the effect of 10 vol.% crystals increases the effective viscosity of sample BL4 by an additional 0.6 log units (Fig. 2). Unlike BL3 and BL6, we were unable to obtain reproducible calorimetry data for BL4. Based on a comparison between peak temperatures at matched heating and cooling rates in the dilatometer, and between calorimetric peaks for BL3 and BL6, we estimate that the physical effect due to the presence of 10 vol.% crystals is 0.3–0.4 log units of viscosity.

Experiments performed on cylinders of melt drilled from within the flow band either perpendicular or parallel to the long axes of microlites (BL4-per and BL4-par in Fig. 2) show no significant difference in apparent vis-

cosity. Any shape factor effect of the microlites on the effective viscosity is within the experimental error (ca. 0.1 log units of viscosity). These viscosity measurements on samples with differing microlite contents demonstrate that rheological complexity due to microlite orientation. Although, the local contrast in viscosity between layers with differing microlite contents and orientation is moderate, the transient rheological effects may be significant and may result in a development of flow bands.

Effect of vesicles in sample BLP

The highest viscosities were obtained for the vesicular pumice from the explosion breccia unit (Fig. 2). To isolate compositional (e.g. H_2O content) from physical effects (e.g. vesicle content) on the viscosity of this vesicular sample, some assumptions need to made. Firstly, because samples from within the Ben Lomond flow have a uniform bulk composition, the composition of the anhydrous made from this pumice glass by remelting at 1650°C is assumed to be similar to the composition of an annealed sample BL6-r. There are difficulties involved in accurately determining water contents of pumice, as glass films between bubbles tend to be thin and prone to hydration. The hydrated sample with 0.5 wt.% water is equivalent to the composition of the melt phase of the pumice. Relative to BL6-r, the effect of 0.5 wt.% water in the melt explains the apparent decrease in viscosity by ~2.6 log units (see Fig. 2). With the viscosity data of the hydrated sample representing the viscosity of the melt in the pumice sample, we conclude that the effect of ca. 50 vol.% of bubbles (with high aspect ratios ~10) at these stresses and strain rates appears to increase the viscosity by ~3.5 log units in comparison with hydrated rhyolite. Obviously, this result is contrary to existing experimental and theoretical data on the rheology of bubble-bearing glasses and melts (Sura and Panda 1990; Bagdassarov and Dingwell 1992; Stein and Spera 1992; Manga et al. 1998). However, Lejeune et al. (1999) also found an increase in shear viscosity of silicate melts for small volume fractions of vesicles (0.03–0.14 vol.%). The explanation of the observed viscosity anomaly of the natural BLP sample is as follows: The melt, initially containing water, has been decompressed and degassed to produce pumice. During the degassing stage, vapour bubbles nucleated and grew in the hydrous melt, contributing water to the vapour phase. This means that there is a thin rim of anhydrous melt surrounding each vesicle in the pumice sample (Stevenson et al. 1997). The contrast in the viscosity between anhydrous rhyolite and rhyolite with the dissolved 0.5 wt.% water is 2.6 log units (this study) and with 1.5 wt.% dissolved water (Stevenson et al. 1997) would be 5.2 log units at temperatures 700–850°C. Effectively, the effect of strained elongated vesicles surrounded by practically elastic shells may result in a shear viscosity increase, which has been observed in experiments with BLP sample. When the concentration of elongated vesicles is close to the so-called touching limit, they may build an elastic "skeleton" structure in the melt and even support some small shear stresses in laboratory experiments. Alternatively, the anomaly in viscosity may be attributed to the explosion-related nature of the sample. Very fast explosive cooling caused nucleation and growth of vesicles at lower temperatures and in a very complicated strained environment. Thus, by annealing the same natural sample, the measured parallel-plate viscosity would be different from relaxed and non-strained foam samples (ca. Bagdassarov and Dingwell 1992). Our data also record that in comparison with the anhydrous glass sample BL6-r, an increase in viscosity of ~1 log unit occurs for BLP.

Some implications for emplacement and cooling of the Ben Lomond dome

Rheological constraints

For understanding the factors which govern the dynamics of the Ben Lomond dome emplacement, an estimation of eruption temperature T_o and lava flow thickness are required.

To constrain the pre-eruptive crystallisation temperature for the essentially aphyric Ben Lomond flow, the one-pyroxene geothermometer of Lindsley (1983) was applied to a pyroxene microphenocryst $Wo_{25–39}$, and a minimum temperature of 900±50°C was obtained. Because some undercooling is required for fast crystallisation of "nano-scale" microlites, we can assume that the calculated temperature is a maximum, with a more realistic temperature being T_o ca. 850°C (Sharp et al. 1996) derived from size distribution of microlites and temperature–nucleation rate relationship. Alternative estimations of the eruptive temperature based on coexisting Fe–Ti oxides in the glass phase in suits of Taupo Volcanic Centre provides ca. 840–850°C (see Fig. 3 in Shane 1998). Comparison against other high silica rhyolites in Taupo Volcanic Centre constrains the pre-eruptive temperature as ca. 800°C (Shane 1998).

For this lava flow, the direct estimation of the lava flow lobe thickness is hampered by a lack of upper obsidian layer (U. OBS; Fig. 1) exposure, due to valley infill between flow lobes by pumice alluvium derived from the 1.8-ka Taupo ignimbrite. The maximum thickness of fine vesicular pumice layer (FVP; Fig. 1) exposed is 6 m, and in some places 10 m thickness has been stripped away by erosion. From morphological analysis, a reasonable estimate of lava flow thickness at the time of eruption and emplacement is ca. 90 m.

The duration L of lava flow emplacement can be estimated with the use of Jeffreys equation (Jeffreys 1925; Nichols 1939) for average flow velocity (v)

$$v = \frac{\rho \cdot g \cdot \sin\theta \cdot h^2}{3 \cdot \eta} \quad (4)$$

by integrating for temperature from the initial emplacement temperature T_o to the final temperature T_g

$$L = \int_{T_g}^{T_0} v \cdot q \cdot dT, \quad (5)$$

where h is the lobe thickness, θ is basement slope, η is the effective shear viscosity, ρ is lava density and q is the average cooling rate between T_o and T_g. The shear viscosity has been taken as an average for BL6 and BL4 samples between T_g and 850°C (Fig. 2). Equation (4) yields an average flow velocity of (10^{-4} m s^{-1}). As the distance between the inferred vent and the toe of each flow lobe is known, emplacement time can be estimated as ca. 1.5 years. Using an equation from Kilburn and Lopes (1991) the upper limit of the emplacement time is ca. 6 years.

No textural evidence has been found for the emplacement of the Ben Lomond flow as a "permeable foam" as advocated by Eichelberger et al. (1986) for some rhyolite domes, in which a magmatic foam is believed to collapse during flow to form obsidian. Instead, the Ben Lomond lava flow is assumed to have erupted as a relatively degassed and poorly vesicular magma, with vesicularity increasing within the upper parts of the flow during flow advance (Stevenson et al. 1994). The minimum eruptive water content, from FTIR analyses, is 0.13 wt.%, with volumetrically minor Cl and F. The measured viscosity of the bubble-free magma between 10 and 40 m depth in the flow at 850°C is between $10^{9.5}$ Pa s for BL6 and 10^{10} Pa s for BL4 (Fig. 2). Lava in the dome would have ceased to flow at temperatures near T_g, when shear viscosity is approximately 10^{12} Pa s. In this temperature range, shear stresses cannot relax by viscous deformation, and strain of the lava dome may occur only via brittle failure. The temperature at the extrapolated viscosity of 10^{12} Pa s is between 700 and 730°C for all measured samples (Table 2). From calorimetric data, the onset of peak temperature is inferred to be 650–680°C giving a lower temperature limit for the emplacement of the Ben Lomond dome (Fig. 3).

Reconstruction of temperature profiles

The simple cooling model described by Manley (1992), based on a one-dimensional solution of the heat transport equation for a horizontal layer, was applied to the Ben Lomond flow. The model takes into account the latent heat of crystallisation, the insulating effect on the upper boundary due to a pumiceous carapace, increased heat loss due to rainfall, and allows the temperature at the basal contact to vary with time from an initial temperature equal to the average of the lava's emplacement temperature and the basement temperature. The model solves only the heat transport equation, and does not take into account the coupling of flow velocity and heat transport, but this effect is minor in cases where flow duration was short compared with cooling time, as was the case for the small Ben Lomond flow. Output from the model may be used as a first approximation for the cooling history of the Ben Lomond lava flow.

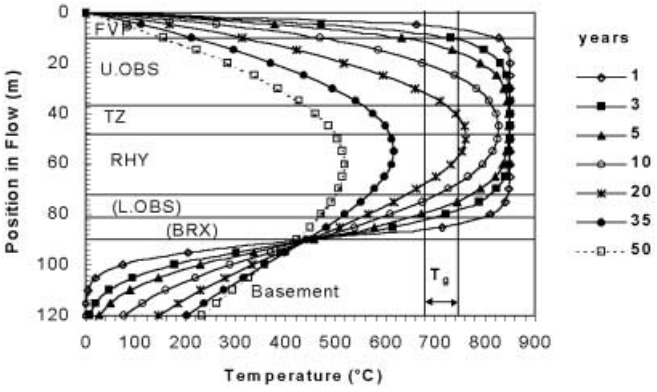

Fig. 4 Temperature profiles of the Ben Lomond flow at time steps of 1, 3, 5, 10, 20, 35 and 50 years, as derived by numerical modelling with the emplacement temperature T_o=850°C. The thickness of the lava flow is assumed to be 90 m. *Horizontal solid lines* demarcate the textural zones observed in the lava flow (Fig. 1). Two additional textural zones (*L. OBS* lower obsidian; *BRX* breccia) are not exposed in the Ben Lomond flow but are inferred to be present as they are in other rhyolite flows (Manley 1992) and are accounted for in the numerical model. The range of the glass transition temperature T_g is shown by the *vertical lines*

Figure 4 represents approximate time–temperature profiles through the southwestern flow lobe ~2 km from the vent for times between 1 and 50 years after emplacement. The calculations assume an emplacement temperature T_o=850°C and a rainfall of 20 cm per annum. The equivalent heat losses due to a rainfall have been subtracted from the heat transport equation for that portion of the upper part of the flow in which T<300°C. The temperature profile changes only slightly when the mean annual precipitation is taken as 50 cm. The temperature profile allows the calculation of cooling rates of ~10^{-6} K s^{-1} for a depth of 10 m and 10^{-7} K s^{-1} at 30 m below the surface. However, uncertainties in the total flow thickness, and in the thickness of the FVP layer, influence the estimated cooling times as shown in Fig. 4.

At a given depth in the flow, the time difference between the beginning of emplacement and the cessation of viscous flow (T_g) provides a first approximation of the length of time available for development of the vesicularity and crystallinity of the various textural units.

Discussion and conclusion

The upper 10 m of the lava flow stratigraphy is typically vesicular, implying that above this depth the vapour pressure in bubbles exceeded the overburden pressure. Dense obsidian occurs at depths where overburden pressure exceeded vapour pressure or where vesiculation was retarded due to a very long nucleation time for vapour bubbles (ca. Bagdassarov et al. 1996). Alternatively, some dense obsidian flows may be formed by a process analogous to welding of a permeable magmatic foam

(Westrich and Eichelberger 1994). The time–temperature profiles in Fig. 4 indicate that after the emergence of the lava flow from the vent, approximately 4 years is required for the upper 10 m (FVP) of the lava flow to cool below the temperature of the brittle–ductile transition. Nucleation and growth of bubbles within the FVP can only occur within this time, when $T>T_g$. Formation of spherulites in the upper obsidian layer can occur within 3–25 years after the emergence of the lava from the vent. In contrast, crystallisation of the groundmass within the central part of the flow (the RHY layer) is permitted to take more than 25 years. The pumice breccia/U. OBS contact at 35 m depth is characterised by flow-deformed vesicles, indicating that the interior of the lava flow remained ductile. In contrast, near the surface, the pumiceous breccia crops out in two dimensions as a fracture-fill deposit cross-cutting both U. OBS and FVP units. These features indicate that formation of the pumice breccia occurred immediately before flow cessation. The pumice breccia near the surface was interpreted previously (Stevenson et al. 1996) as a cross section through an infilled explosion pit. The pumice breccia has a sharp contact, with angular fragments of spherulitic black obsidian within brown fractured and perlitised glassy groundmass. This field evidence suggests that the explosion pit formed after the upper part of the flow cooled below T_g, up to 3 years after the lava emerged from the vent. In contrast, the interior of the flow (e.g. the pumiceous pod at 30 m depth) could have remained ductile for up to 15–20 years after flow emplacement. Slow cooling of the lava flow interior caused it to remain at a lower viscosity for a longer period of time than the flow carapace. If a tension crack propagating downwards into the flow were to intersect a volatile-rich pocket within the upper obsidian layer, gas decompression could result in the formation of an explosion pit, long after the upper several metres of the lava flow had cooled below T_g.

Using Fig. 4 and the Arrhenian temperature dependence of the viscosity (Fig. 2), time–viscosity profiles were also constructed for the first 8 years of the flow's cooling history (Fig. 5). As the flow's emplacement duration was between 1.5 and 6 years (see above), viscosity data for crystallite-poor sample BL6, which would have passed through T_g at approximately 5–6 years after eruption, was used to calculate the time–viscosity structure of the entire upper 40 m of the flow. The greater crystal contents of the deeper samples (BL3 and BL4) would have developed over a time period longer than the emplacement duration.

The textural characteristics and viscosity of the breccia body (BLP) centred at 35 m depth provide important insights into the state and activity of the Ben Lomond lava flow during emplacement. The breccia material's lack of microlites indicates that it formed before slow cooling could cause crystals to nucleate and grow, and also indicates that breccia formation likely caused "freezing" of the breccia material by explosive loss of water vapour and the resultant displacement of the material's solidus to higher temperatures. The loss of water then allowed

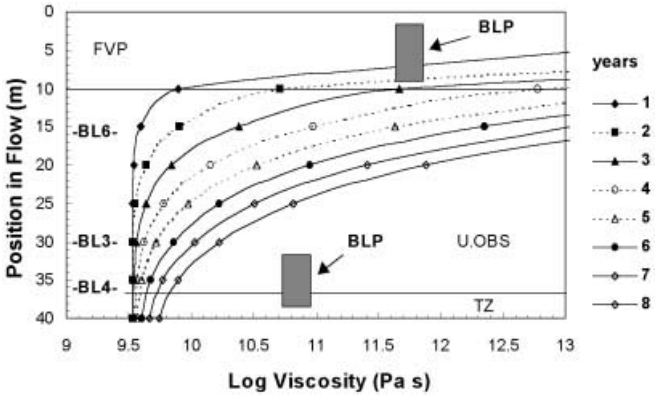

Fig. 5 Viscosity profiles at time steps of 1 through 8 years, estimated on the basis of the rheological measurements of Ben Lomond sample BL6, BL3, BL4 and the temperature profiles plotted in Fig. 4. The *rectangles* show the viscosities of the explosion breccia bodies BLP, calculated for a time step of 1 year. The deeper breccia body apparently developed viscosities much higher than the surrounding lava due to presence of vesicles caused by explosive decompression

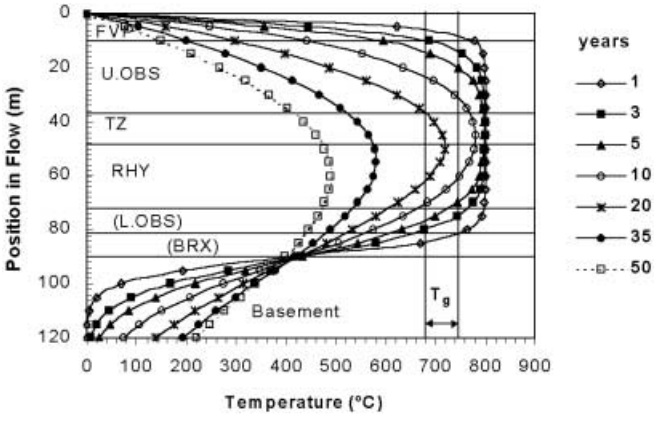

Fig. 6 Temperature profiles of the Ben Lomond flow at time steps of 1, 3, 5, 10, 20, 35 and 50 years, as derived by numerical modelling with the emplacement temperature T_o=800°C

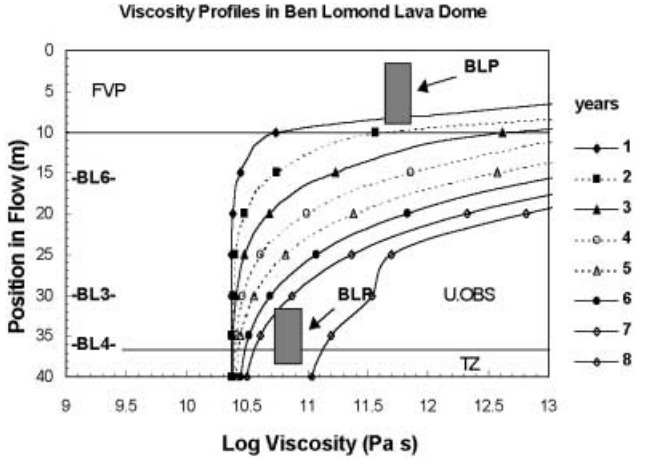

Fig. 7 Viscosity profiles at time steps of 1 through 8 years, estimated on the basis of the rheological measurements of Ben Lomond sample BL6, BL4, BL3 and the temperature profiles plotted in Fig. 6

the breccia to remain microlite-free even as it cooled at approximately the same rate as the surrounding lava, as represented by BL4 with up to 10 vol.% microlites.

Figure 5 also shows that local explosive decompression events early in the lava flow's cooling history can significantly change its local viscosity structure and thus influence it flow dynamics. Flow velocity might also be affected if breccia formation involved a substantial percentage of a given portion of a lava flow.

For comparison, the results of cooling model with the emplacement temperature T_o=800°C and time–viscosity profiles for the first 8 years of the flow's cooling history are shown in Figs. 6 and 7, respectively. Lower pre-eruptive temperature means higher viscosity and shorter time before the flow ceased to flow.

References

Anderson SW, Fink JH (1990) The development and distribution of surface textures at Mount St. Helens dome. IAVCEI Proc Volcanol 2:25–46

Anderson SW, Fink JH (1992) Crease structures: indicators of emplacement rates and surface stress regimes of lava flows. Geol Soc Am Bull 104:615–625

Anderson SW, Fink JH, Rose WI (1995) Mount St. Helens and Santiaguito lava domes: the effect of short-term eruption rate on surface texture and degassing processes. J Volcanol Geotherm Res 69:105–116

Bagdassarov NS, Dingwell DB (1992) A rheological investigation of vesicular rhyolite. J Volcanol Geotherm Res 50:307–322

Bagdassarov NS, Dingwell DB, Wilding MC (1996) Rhyolite magma degassing: an experimental study of melt vesiculation. Bull Volcanol 57:587–601

Cook GB, Cooper RF (2000) Iron concentration and the physical processes of dynamic oxidation in an alkaline earth aluminosilicate glass. Am Mineral 85:397–406

Dingwell DB (1995) Relaxation in silicate melts: some applications. MSA Rev Mineral 32:21–66

Dingwell DB, Bagdassarov NS, Bussod GY, Webb SL (1993) Magma rheology. In: Luth RW (ed) Experiments at high pressures and applications to the Earth's mantle. Mineral Association of Canada, Edmonton, pp 131–196

Dingwell DB, Romano C, Hess K-U (1996) The effect of water on the viscosity of a haplogranitic melt under P–T–X conditions relevant to silicic volcanism. Contrib Mineral Petrol 124:19–28

Eichelberger JC, Carrigan CR, Westrich HR, Price RH (1986) Non-explosive silicic volcanism. Nature 323:598–602

Fink JH (1983) Structure and emplacement of a rhyolitic obsidian flow, Little Glass Mountain, N. California. Geol Soc Am Bull 94:362–380

Fink JH, Manley CR (1989) Explosive volcanic activity generated from within advancing silicic flows. IAVCEI Proc Volcanol 1:169–179

Fink JH, Anderson SW, Manley CR (1992) Textural constraints on effusive silicic volcanism: beyond the permeable model. J Geophys Res 97:9073–9083

Fontana E (1970) A versatile parallel-plate viscometer for glass viscosity measurements to 1000°C. Ceramic Bull 49:594–597

Gent AN (1960) Theory of the parallel plate viscosimeter. Br J Appl Phys 11:85–88

Hess K-U, Dingwell DB (1996) Viscosities of hydrous leucogranitic melts: a non-Arrhenian model. Am Mineral 81:1297–1300

Jeffreys H (1925) The flow of water in an inclined channel of rectangular section. Phil Mag 49:793–807

Jousset P, Okada H (1999) Post-eruptive volcanic dome evolution as revealed by deformation and microgravity observations at Usu volcano (Hokkaido, Japan). J Volcanol Geotherm Res 89: 255–273

Kilburn CR, Lopes RMC (1991) General patterns of flow field growth: Aa and blocky lavas. J Geophys Res 96:19721–19732

Lejeune AM, Bottinga Y, Trull TW, Richet P (1999) Rheology of bubble-bearing magmas. Earth Planet Sci Lett 166:71–84

Lindsley DH (1983) Pyroxene thermometry. Am Mineral 68:477–493

Manga M, Castro J, Cashman KV, Loewenberg M (1998) Rheology of bubble-bearing magmas. J Volcanol Geotherm Res 87:15–28

Manley CR (1992) Extended cooling and viscous flow of large, hot rhyolitic lavas: implications of numerical modelling results. J Volcanol Geotherm Res 53:27–46

Manley CR (1996) Physical volcanology of a voluminous rhyolite lava flow: the Badlands lava, Owhyee Plateau, southwestern Idaho. J Volcanol Geotherm Res 71:129–153

Matthews SJ, Gardeweg MC, Sparks RSJ (1997) The 1984 to 1996 cyclic activity of Lascar Volcano, northern Chile: cycles of dome growth, dome subsidence, degassing and explosive eruptions. Bull Volcanol 59:72–82

Mothes PA, Hall ML, Janda RJ (1998) The enormous Chillos Valley Lahar: an ash-flow-generated debris flow from Cotopaxi Volcano, Ecuador. Bull Volcanol 59:233–244

Newman S, Stolper EM, Epstein S (1986) Measurements of water in rhyolitic glasses: calibration of an infrared spectroscopic technique. Am Mineral 71:1527–1541

Nichols BL (1939) Viscosity of lava. J Geol 47:290–302

Pocklington HC (1940) Rough measurements of high viscosities. Proc Cambridge Phil Soc 36:507–508

Richet P, Lejeune A-M, Holtz F, Roux J (1996) Water and the viscosity of andesite melts. Chem Geol 128:185–197

Richter DH, Moll-Stalcup EJ, Miller TP, Lanphere MA, Dalrymple GB, Smith RL (1994) Eruptive history and petrology of Mount Drum volcano, Wrangell Mountains, Alaska. Bull Volcanol 56:29–46

Roux J, Holtz F, Lefèvre A, Schulze F (1994) A reliable high-temperature setup for internally heated pressure vessels: applications to silicate melt studies. Am Mineral 79:1145–1149

Scaillet B, Holtz F, Pichavant M, Schmidt M (1996) The viscosity of Himalayan leucogranites: implication for mechanisms of granitic magma ascent. J Geophys Res 101:27691–27699

Scherer GW (1984) Relaxation in glass and composites. Wiley, New York

Schulz F, Behrens H, Holtz F, Roux J, Johannes W (1996) The influence of H2O on the viscosity of a haplogranitic melt. Am Mineral 81:1155–1165

Shane P (1998) Correlation of rhyolitic pyroclastic eruptive units from the Taupo volcanic zone by Fe–Ti oxide compositional data. Bull Volcanol 60:224–238

Sharp T, Stevenson RJ, Dingwell DB (1996) Microlites and "nanolites" in rhyolitic glass: microstructural and chemical characterisation. Bull Volcanol 57:631–640

Sparks RSJ (1997) Causes and consequences of pressurisation in lava dome eruption. Earth Planet Sci Lett 150:177–189

Stein DJ, Spera FJ (1992) Rheology and microstructure of magmatic emulsions: theory and experiments. J Volcanol Geotherm Res 49:157–174

Stevenson RJ, Briggs RM, Hodder APW (1994) Physical volcanology and emplacement history of the Ben Lomond rhyolite lava flow, Taupo Volcanic Centre, New Zealand. NZ J Geol Geophys 37:345–358

Stevenson RJ, Dingwell DB, Webb SL, Bagdassarov NS (1995) The equivalence of enthalpic and shear-stress relaxation in rhyolitic obsidians and quantification of the liquid–glass transition in volcanic processes. J Volcanol Geotherm Res 68:297–306

Stevenson RJ, Dingwell DB, Webb SL, Sharp TG (1996) Viscosity of microlite-bearing rhyolitic obsidians: an experimental study. Bull Volcanol 58:298–309

Stevenson RJ, Bagdassarov NS, Romano C (1997) Vesiculation processes in a water-rich calc-alkaline obsidian. Earth Planet Sci Lett 146:555–571

Stevenson RJ, Bagdassarov NS, Dingwell DB, Romano C (1998) The influence of trace amounts of water on the viscosity of rhyolites. Bull Volcanol 60:89–97

Stolper EM (1982) Water in silicate glasses: an infrared spectroscopic study. Contrib Mineral Petrol 81:1–17
Sura VM, Panda PC (1990) Viscosity of porous glass. J Am Ceram Soc 73:2697–2701
Swanson DA, Holcomb RT (1990) Regularities in growth of the Mount St. Helens dacite dome 1980–1986. IAVCEI Proc Volcanol 2:1–24
Tobolsky AV, Taylor RB (1962) Viscoelastic properties of a simple organic glass. J Phys Chem 67:2439–2442
Wadge G, Francis PW, Ramirez CF (1995) The Socompa collapse and avalanche event. J Volcanol Geotherm Res 66:309–336
Watanabe K, Danhara T, Watanabe K, Terai K, Yamashita T (1999) Juvenile volcanic glass erupted before the appearance of the 1991 lava dome, Unzen volcano, Kyushu, Japan. J Volcanol Geotherm Res 89:113–121
Webb SL, Dingwell DB (1990a) Non-Newtonian rheology of igneous melts at high stresses and strain rates: experimental results for rhyolite, andesite, basalt and nephelenite. J Geophys Res 95:15695–15701
Webb SL, Dingwell DB (1990b) The onset of non-Newtonian rheology in silicate melts. Phys Chem Mineral 17:125–132
Westrich HR (1987) Determination of water in volcanic glasses by Karl-Fischer titration. Chem Geol 63:335–340
Westrich HR, Eichelberger JC (1994) Gas transport and bubble collapse in rhyolitic magma: an experimental approach. Bull Volcanol 56:447–458
Westrich HR, Stockman HW, Eichelberger JC (1988) Degassing of rhyolitic magma during ascent and emplacement. J Geophys Res 93:6503–6511
Yamashina K, Shimizu H (1999) Crustal deformation in the mid-May 1991 crisis preceding the extrusion of a dacite lava dome at Unzen volcano, Japan. J Volcanol Geotherm Res 89:43–55